Arch. Metall. Mater. **70** (2025), 2, 701-713

DOI: https://doi.org/10.24425/amm.2025.153471

RUPENDRA S. TANWAR[1], SUYOG JHAVAR[1*]

# EFFECT OF HEAT TREATMENT ON THIN WALL OF BIMETALLIC AUSTENITIC STEEL FABRICATED THROUGH WIRE ARC ADDITIVE MANUFACTURING (WAAM)

Wire and Arc Additive Manufacturing (WAAM) enables the fabrication of complex geometrical features and intricate components. SS316L is favoured for its superior corrosion resistance and mechanical strength. However, WAAM-fabricated SS316L components are prone to hot cracking due to their fully austenitic microstructure. Conversely, SS309, with its higher ferritic content, has shown potential in mitigating hot cracking when alloyed with SS316L. In this study, bimetallic SS316L-SS309 thin wall was fabricated using WAAM and subjected to heat treatments at 400°C, 950°C, and 1200°C, each for a duration of two hours, to investigate the resultant effects on microstructural evolution and mechanical properties. The as-built specimens exhibited δ-ferrite dendrites within an austenitic ($\gamma$) matrix, with finer grain structures compared to heat-treated samples. Minimal changes were observed in microstructure and mechanical properties at 400°C, while treatments at 950°C and 1200°C resulted in a significant reduction in ultimate tensile strength (UTS), accompanied by nearly double the elongation for samples treated at 1200°C relative to their as-deposited counterparts whereas 14.3% reduction in UTS, Whereas the hardness decrease by 25-35 HV. This study highlights the impact of heat treatment on the microstructural stability and mechanical performance of WAAM-fabricated thin bimetallic austenitic steel structures.

*Keywords:* Additive manufacturing; Austenitic steel; WAAM; Bimetallic structure; heat treatment

## 1. Introduction

Additive Manufacturing (AM) has made remarkable progress since the inception of the first 3D printer, radically altering the manufacturing industry and creating new opportunities. Over the last twenty years, metal additive manufacturing (AM) techniques have developed, allowing for the creation of metal components using powdered, wired, or sheet materials [1]. Unlike traditional manufacturing methods like machining, casting, or forging, additive manufacturing (AM) constructs things by incrementally adding material layer by layer, without the need for any tools. This technique enables the creation of intricate geometries that cannot be achieved by conventional manufacturing procedures. Several research in the literature investigate different additive manufacturing (AM) procedures that employ heat sources such as electron beams, lasers, or electrical arcs [2,3]. Powder Bed Fusion (PBF) utilizes lasers or electron beams to selectively melt small layers of powder, each measuring less than 100 μm. This process enables the production of intricate parts with great complexity. However, it is important to note that PBF is limited by size limits [4-6]. The process of fabricating even modest pieces for the PBF needs a significant amount of time. On the other hand, Direct Energy Deposition (DED) use electron beams, lasers, or electrical arcs to generate a molten pool using powder or wire. This method allows for a faster construction rate, making it possible to produce larger and less complex components at a lower cost [7]. Kladovasilakis et al. conducted a comparison between powder bed fusion (PBF) and powder-directed energy deposition (powder-DED) techniques with wire-directed energy deposition (wire-DED), emphasizing that wire-DED, also known as wire arc additive manufacturing (WAAM), achieves a faster building speed. This enables the production of large component almost finished objects that may need additional machining or grinding for surface refinement. In addition, laser and electron beam devices are expensive and require a significant amount of time, which makes them better suited for manufacturing high-value components [8]. The conventional welding methods such as Plasma arc welding (PAW), gas metal arc welding (GMAW) and gas tungsten arc welding (GTAW) used as heat source to melt the welding wire. various

[1] VIT-AP UNIVERSITY, DEPARTMENT OF MECHANICAL ENGINEERING, AMRAVATHI, ANDHRA PRADESH, INDIA, 522241

* Corresponding author: suyogjhavar@gmail.com

© 2025. The Author(s). This is an open-access article distributed under the terms of the Creative Commons Attribution License (CC-BY 4.0). The Journal license is: https://creativecommons.org/licenses/by/4.0/deed.en. This license allows others to distribute, remix, modify, and build upon the author's work, even commercially, as long as the original work is attributed to the author.

metal wires, including Titanium alloys (Ti6Al4V), superalloys (IN718), aluminium alloys (AlSi10Mg) and stainless steels (SS316L) [9-11].

Owing to its high temperature resistance, excellent corrosion resistance, weldability, high strength and creep resistance, 316L austenitic steel is widely used in the manufacturing of parts intended for use in highly corrosive environment such as impeller, blade and valve [12]. Recently C Nota et al., [13] highlighted that the propeller is critical component in naval applications and proposed that WAAM could serve as a viable alternative for producing high quality components, thereby reinforcing this essential link in the supply chain. Additionally, using the WAAM process for propeller manufacturing would enable complete repairability throughout their life cycle, unlike traditional casting methods. This approach reduces costly spare part inventory and minimizes ship downtime. On the other hand, SS309 contains higher chromium (22-25 wt.%) and Nickel (12-14 wt.%) as compared to SS316L, making it preferred choice for the joining of stainless steel to other dissimilar metals specifically in naval ship building and repairs [14]. The elevated chromium content promotes ferrite formation which increase resistance to corrosion and oxidation [15,16]. In contrast, the presence of nickel promotes the formation of austenite which increase ductility and high temperature strength. The elevated ferrite content in SS309 reduces the tendency of hot cracking during repair of SS316L propellers [17,18]. This remanufacturing approach creates a bimetallic structure of SS316L and SS309. Component composed of two different materials that meet specific application requirements are of significant interest, making bimetallic components a prominent area of research. Bimetallic materials can integrate the distinct performance characteristics of each constituent material, resulting in locally tailored properties that enhance the material's overall functionality [19]. Powder metallurgy, casting, welding, and forging are the conventional methods to fabricate bimetallic components [20-23].

Although WAAM offers several advantages, it is also accompanied by notable drawbacks. The high heat input and the continuous thermal cycling of heating and cooling on each layer induce residual stresses and lead to anisotropy in the microstructure and mechanical properties. In the case of components fabricated from SS316L and SS309 using WAAM, a notable presence of ferritic phases is observed due to the transformation from austenite to ferrite during the solidification process [24]. Chen et al. [25] conducted a study on WAAM 316L stainless steel and found that heat treatments conducted at temperatures between 1000°C and 1200°C for 1 hour primarily altered the volume fractions of the $\sigma$ and $\delta$ phases. However, treatment at 1200°C for 4 hours led to significant grain coarsening and a transition from a columnar to an equiaxial grain structure. The study also observed that an increase in the $\sigma$ phase fraction was associated with enhanced ultimate tensile strength (UTS) and yield strength (YS), but a reduction in elongation (El) and reduction of area (RA). Conversely, after the complete elimination of $\sigma$ and $\delta$ phases, both UTS and YS were reduced, while El and RA improved. Nonetheless, heat treatment of bimetallic AM components presents critical challenges, including the need to address differences in optimal heat treatment conditions for each material and their miscibility. Additionally, the diffusion of elements at the interface and the formation and growth of intermetallic phases during the heat treatment process must be thoroughly investigated.

In this paper, a detailed investigation into the effects of heat treatment on a thin wall of austenitic bimetallic structure (BMS) is presented, focusing on microstructural and mechanical property analysis. Utilizing a WAAM setup developed by the research group, the BMS was fabricated by sequentially depositing SS316L and SS309 layers. Although no critical defects were observed, heat treatments were conducted at 400°C, 950°C, and 1200°C, with these specific temperatures selected based on existing literature [26,27]. The microstructure and composition were characterized using optical and electron microscopy, along with elemental mapping techniques. Additionally, microhardness and tensile tests were carried out, including the identification and analysis of fracture locations and surfaces. The study reveals the mechanisms underlying the observed improvements and proposes near-optimal heat-treatment parameters for the BMS.

## 2. Materials and methods

### 2.1. Materials and manufacturing process

The experimental setup consists of 3-Axis computer numerical control (CNC), GMAW controller, welding torch, wire feeder, shielding gas, and CNC controller Shown in Fig. 1(a) and the sample fabrication strategy mentioned in Fig. 1(b). The welding torch mounted on the vertical Z-axis spindle which is perpendicular to the substrate which was clamped on the X-axis working table using C-clamps. The stand-off distance maintained 8-10 mm for each successive layer. The movement of all three-axis control through CNC controller, which operates according to the programme fed into it based on the specific requirements. The wire spool is mounted on the wire feeder carriage and the speed of wire 5 mm/sec, voltage 18.18 V, and current 110 Ampere control through GMAW controller. GMAW is most preferred welding equipment because the wire acts as both filler wire material and electrode. Additionally, the pure (99.99%) shielding gas (Argon) pipe fastened with welding gun and gas is supplies 18-20 $Lmin^{-1}$ during arc generation, protecting the deposited layer from oxidation and agitating the unsolidified molten pool. A 9-array design of experiment (DoE) approach was used to optimize the process parameters, optimal parameters shown in TABLE 1. In this study, bimetallic wall was fabricated using WAAM as illustrated in Fig. 1(a) and the deposition strategy as shown in Fig. 1(b). A dwell time 60-120 seconds was provided between each layer to ensure optimal interlayer adhesion. The approximate dimension of the thin wall is 120 mm × 6 mm × 60 mm (Length × width × height). The fabrication involved depositing 10 layers of SS316L on a SS316L substrate, followed by 10 layers of SS309 and then 10 layers of SS316L using commercially

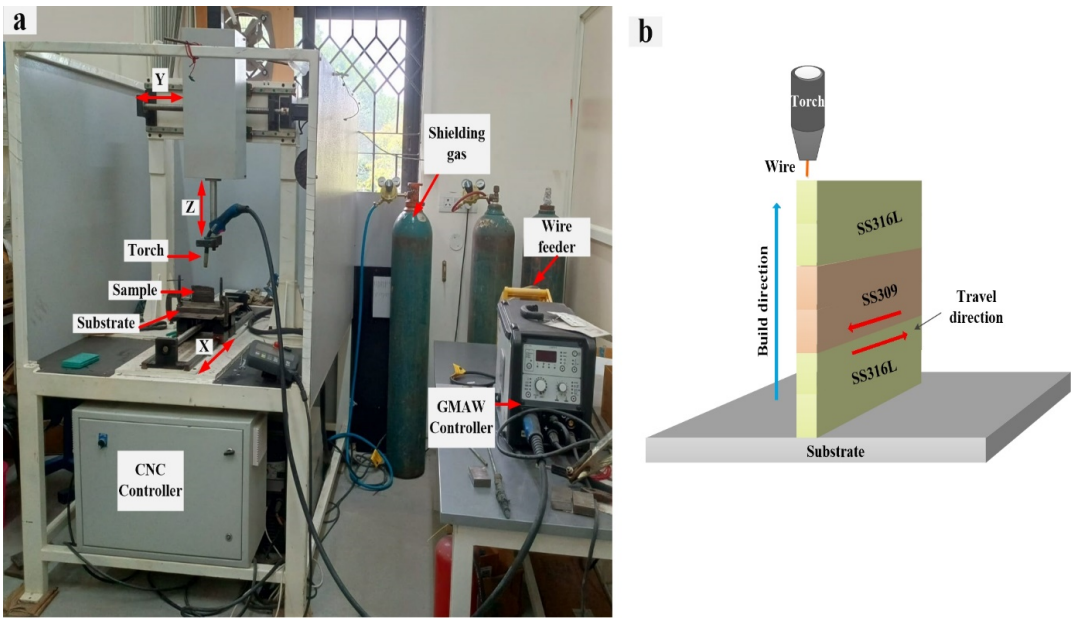


Fig. 1. (a) The experimental setup used for fabrication, (b) The fabrication strategy

available 316L and SS309 wires, with each diameter of 0.8 mm. The chemical compositions of these welding wires are detailed in TABLE 2. Three distinct heat treatment conditions shown in Fig. 2 were applied as follows:

1. The initial heat treatment (HT) involved stress relief at 400°C for 1 hour.
2. A second HT was designed to promote sigma phase precipitation, carried out at 950°C for 2 hours, followed by water quenching.
3. A third HT was conducted at 1200°C for 2 hours, also followed by water quenching.

In all cases, the samples were heated to the target temperature at a rate of 20°C/s. Cooling conditions varied: the first heat treatment (case 1) employed a cooling rate of 5°C/s, whereas the remaining heat treatments utilized a cooling rate of 20°C/s. The heat treatment conditions mentioned in the Fig. 2.

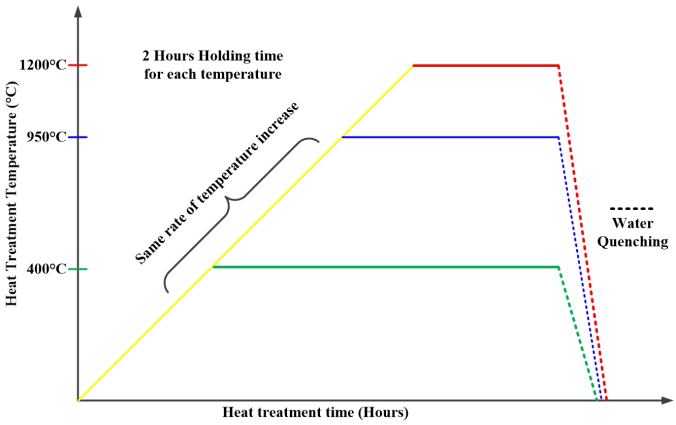


Fig. 2. Graphical representations of heat treatment conditions

### 2.2. Microstructural characterization

The WAAM schematic shown in Fig. 3(a) and the fabricated sample shown in Fig. 2(b). The wire cut electro discharge machine (EDM) was used to extract the samples from the WAAM-fabricated sample at the locations mentioned in the Fig. 3(c). The microstructural investigation of both the as deposited and heat-treated samples involved a range of techniques, such as optical microscopy (OM), scanning electron microscopy (SEM). Optical microscopy was used to examine the microstructure of the samples. The surface morphology was characterized using

TABLE 1

Optimal process parameters

| Voltage (V) | Current (A) | Wire feed rate (mm/sec) | Torch travel speed (mm/min) | Shielding gas flow rate ($Lmin^{-1}$) | Interlayer cooling time (sec) |
|---|---|---|---|---|---|
| 18.18 | 110 | 5 | 400 | 20 | 60-120 |

TABLE 2

Chemical composition (in wt.%) of SS 316 L and SS309 consumable wires

| | C | Mn | Si | S | P | Cr | Ni | Mo | Fe |
|---|---|---|---|---|---|---|---|---|---|
| **SS316L** | 0.03 | 2.21-3.9 | 0.30-0.45 | 0.02 | 0.02 | 18.70-20.20 | 9.9-12.0 | 2.43-3.33 | Balance |
| **SS309** | 0.03 | 1-2.5 | 0.25 | 0.03 | 0.03 | 23-25 | 12-14 | 0.75 | Balance |

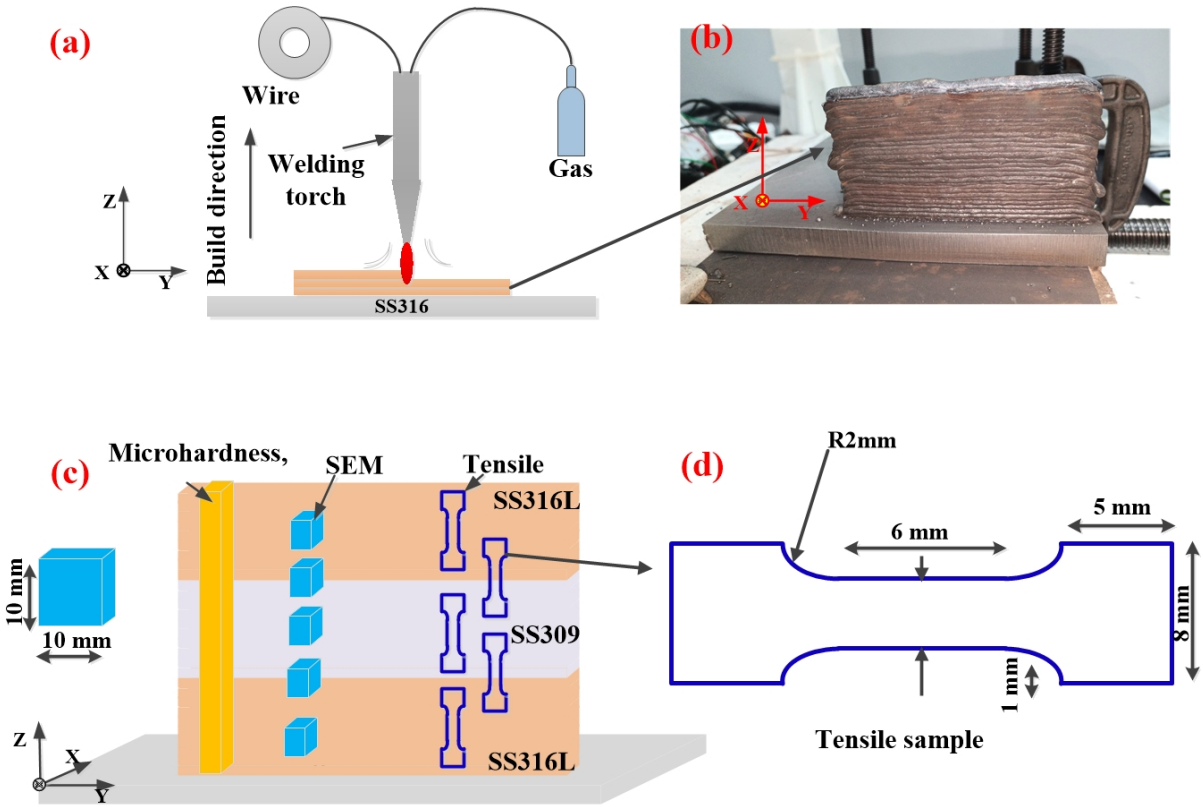


Fig. 3. (a) WAAM Schematic, (b) fabricated WAAM sample, (c) The characterization samples extracted from the WAAL, (d) Tensile sample dimensions as per ASTM E8 [refrence]

Scanning Electron Microscopy (SEM, EVO-18 ZEISS). In order to examine the microstructure morphology, the samples underwent a polishing process until a reflective surface was achieved. Subsequently, the samples were treated with Nital reagent, which consists of 10 ml of nitric acid and 100 ml of ethanol, for etching purposes. This extensive metallographic characterisation procedure enables a thorough analysis of the microstructure and characteristics of the sample, offering significant insights into its original state and its condition after undergoing heat treatment.

### 2.3. Mechanical testing

Tensile test specimens were extracted from the as-built fabricated sample using wire-cut electrical discharge machining (Make: Electronica, Model: ES300). Specimens were prepared in both the build (vertical) and deposition (horizontal) directions of the manufactured bimetallic component, specifically at the interface, while vertical samples were taken from the base metals. A total of fifteen tensile specimens (as deposited and heat treated) were tested using a universal tensile testing machine (Make: TiniusOlsen, UK; Model: 10ST), with three samples from each interface in both the build and deposition directions, and one vertical specimen each from SS316L and SS309 and the mean values are selected for creating the graph. The vertical specimens had the interface positioned at the midpoint of the gauge length, whereas the horizontal specimens had the interface aligned parallel to the tensile axis. The dimensions of the tensile specimens are illustrated in Fig. 3(d). Tensile tests were performed at a crosshead speed of 2 mm/min at room temperature (25±3°C). Each tensile property was tested three times under each condition to ensure repeatability, with the average values reported. Hardness measurements were conducted using a Vickers's micro-hardness Testing Machine, applying a load of 0.5 kg for 10 seconds across the entire height of the sample before and after heat treatment, with indentations spaced 500 µm apart. SEM were employed for fractography to analyze the tensile failure process.

## 3. Results and discussions

### 3.1. Mechanical properties of as-deposited BS

The uniaxial tensile strength of WAAM-printed bimetallic SS316L-SS309 wall structures was investigated along both the build and deposition directions using a universal testing machine (TiniusOlsen H10 KL) with a force capacity of 10 kN. Three samples were tested to ensure repeatability and reliability of results, providing an average tensile strength for both WAAM-built and conventionally manufactured steel samples. The tensile stress versus strain curves for the tested bimetallic WAAM-built structures performed and the comparison of the yield strength (YS), ultimate tensile strength (UTS), and elongation (EL) shown in Fig. 4. The results indicate that the bimetallic WAAM-built structures of SS316L-SS309 along the build direction (SS316L-SS309V and SS309-SS316LV)

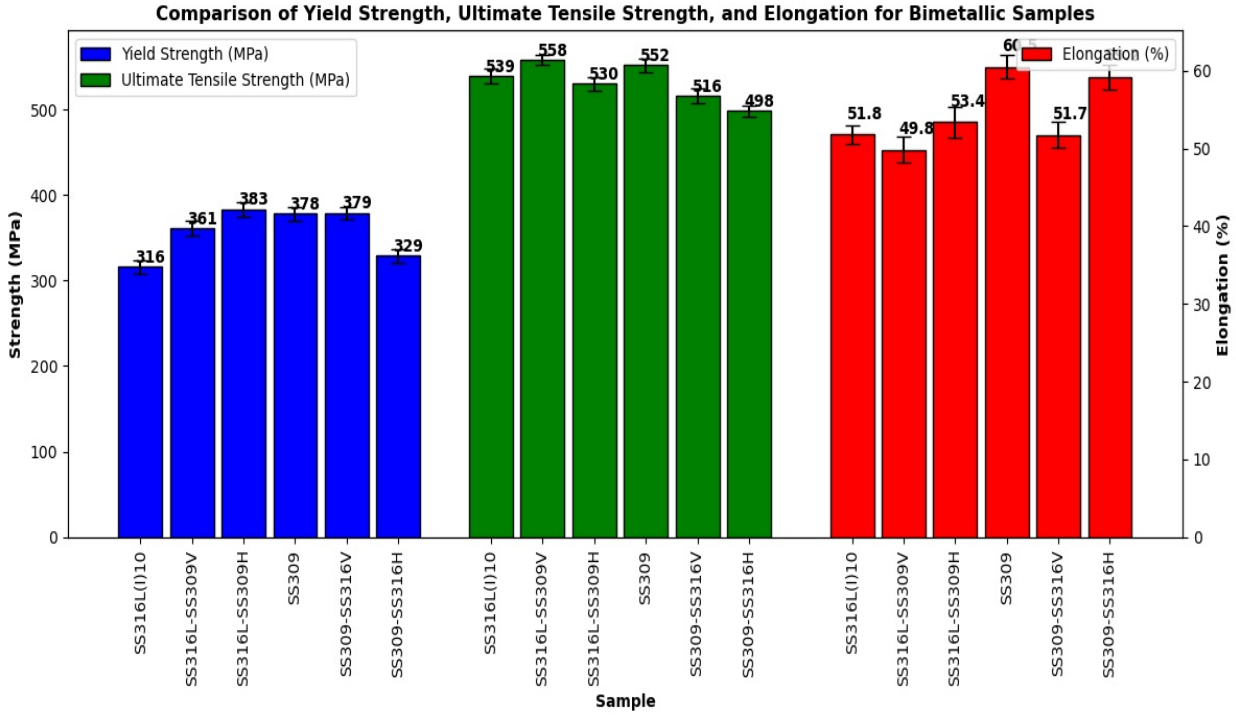


Fig. 4. Mechanical properties of bimetallic structure (BMS) SS316L-SS309 WAAM sample

exhibit relatively higher tensile strength and ductility compared to the base materials SS316L and SS309. Conversely, samples tested along the deposition direction (SS316L-SS309H and SS309-SS316L H) displayed lower tensile strength compared to the base materials. The tensile characteristics of the bimetallic structure discussed earlier have shown a significant change due to variations in its microstructure. The SS316L(I)10 demonstrated a mean YS of 316±3.89 MPa, an UTS of 539.73±2.75 MPa, and an EL of 51.80±1.9% in the direction of construction. On the other hand, the SS 309 exhibited an average yield strength of 378±4.16 MPa, UTS of 552±1.89 MPa, and EL of 60.5±1.21% in the same direction. The interface samples were taken from the build direction (SS316L-SS309V) and deposition direction (SS316L-SS309H). The samples from the build direction demonstrated an enhancement in both the average yield strength and ultimate tensile strength. While there is no noticeable improvement found in the deposition directions for the initial interface. Nevertheless, there was no notable decrease in the percentage of elongation values, as both materials are part of the austenitic steel family. However, the results indicate that the transverse direction sample exhibited greater elongation compared to the construct direction sample. The plastic straining occurred exclusively in the SS316L material as a result of a disparity in strength between the two materials. This caused a build-up of plastic strain, leading to strain localization, namely in the lower tensile strength SS309 portion of the vertical tensile specimen composed of two different materials. The literature also addressed the impact of strength mismatch on the deformation and fracture behaviors of interface and weld situations. Therefore, the designer must be cognizant of the decrease in the overall ability to stretch under stress. Bi-material additive manufacturing (WAAM) systems with mismatched properties experience tensile loading perpendicular to the interface. However, notable discrepancies in the YS, UTS, and EL values were noted between the vertical and horizontal samples. The enhanced strength and reduced ductility were ascribed to the presence of the ferrite phase at the bimetallic interface, as elucidated in earlier sections. The fracture on the side of SS316L indicated that the tensile strength at the interface and SS309 side was greater than that of the SS316L side, and the two alloys exhibited good bonding at the interface. The fracture in the horizontal direction manifested at the interface, so verifying that the average values of UTS and YS in the horizontal direction exceeded those in the vertical direction. The fracture positions of the bimetal specimens were determined based on the UTS value of the SS316L side material. The abrupt rise in the yield and tensile strength measurements of the interface specimens, transitioning from the horizontal sample to the vertical one, can be attributed to a greater presence of alpha ferrite along the interface, as elaborated upon in the microstructure section. These results indicate lower anisotropic behavior in mechanical properties along the build direction compared to the deposition direction. The study observed an enhancement in ultimate tensile strength, with values exceeding those specified by ASTM A312 for SS316L, meeting industrial application standards [28]. The variations in tensile properties of the WAAM-printed bimetallic structures are primarily attributed to heterogeneous microstructural changes resulting from the multiple heating and cooling cycles during fabrication as well as the slightly variations in the chemical composition [29].

The interface region of SS316L-SS309 within the WAAM-built structure demonstrates greater mechanical strength due to the increased ferrite phase which restricts grain movement at the

interface. Whereas, the SS309 sample failed the approximately in the middle of gauge length due to uniform microstructure observed there, this result is consistent published studies [24]. The SS316L-SS309 V interface region demonstrated higher yield strength, corroborating finding from similar kind of study conducted by kesarwani et al. [30].

### 3.2. Optical and SEM for as deposited BMS

In the as-deposited BMS sample, in this study SS316L and SS309, composed primarily of Fe, Cr, and Ni, along with other elements. The optical micrographs of SS316L, illustrating its grain structure, are presented in Fig. 5(a-d). The average grain size was measured to be approximately 21 µm. The microstructure of SS316L predominantly consists of austenite with a face-centered cubic (FCC) lattice, along with delta ferrite exhibiting a body-centered cubic (BCC) structure. Delta ferrite appears as darker regions within the brighter austenite matrix. In comparison, SS309 contains a higher concentration of ferrite-promoting elements, which enhances ferrite formation within the austenitic phase, thereby reducing susceptibility to hot cracking. The interface between SS316L and SS309 is approximately 50 µm in width. Both SS316L and SS309 display a mixture of equiaxed and columnar dendritic structures, as shown in Fig. 5(a-d).

The microstructure analysis of SS316L and SS309 WAAM bimetallic walls reveals distinct morphological characteristics due to variations in their chemical compositions and thermal histories shown in Fig. 6(a-f). In both alloys, the $\delta$ phase appears with a fine vermicular morphology embedded within the $\gamma$ phase matrix. Notably, SS316L exhibits coarser grains relative to SS309, attributed to differences in elemental composition. The microstructure of SS309 shows a higher content of $\delta$ ferrite due to its increased concentration of ferrite-stabilizing elements (Cr, Ni,Mo), leading to a greater presence of ferrite phases compared to SS316L. At the interface between SS316L and SS309 regions, an elevated amount of $\delta$ ferrite is observed, which partially re-dissolves into the $\gamma$ phase under the influence of subsequent thermal cycles. The retained $\delta$ phase maintains a vermicular morphology within the austenitic matrix. Additionally, high interlayer temperatures result in the formation of numerous small pores (dark circular structures) within the $\gamma$ matrix. The microstructure transitions also produce a mix of equiaxed grains and cellular dendrites, with SS309 exhibiting finer grain structures than SS316L, primarily due to its higher content of ferrite-stabilizing elements. These microstructural variations have significant implications for the mechanical properties and performance of the bimetallic structures in additive manufacturing applications.

The XRD analysis of Wire Arc DED-fabricated SS316L, SS309, and the bimetallic SS316L-SS309 structure (BMS) reveals phase transformations induced by the thermal cycles inherent in the process (see Fig. 7). The dominant diffraction peaks at (111), (200), (220), and (311) confirm the presence of the

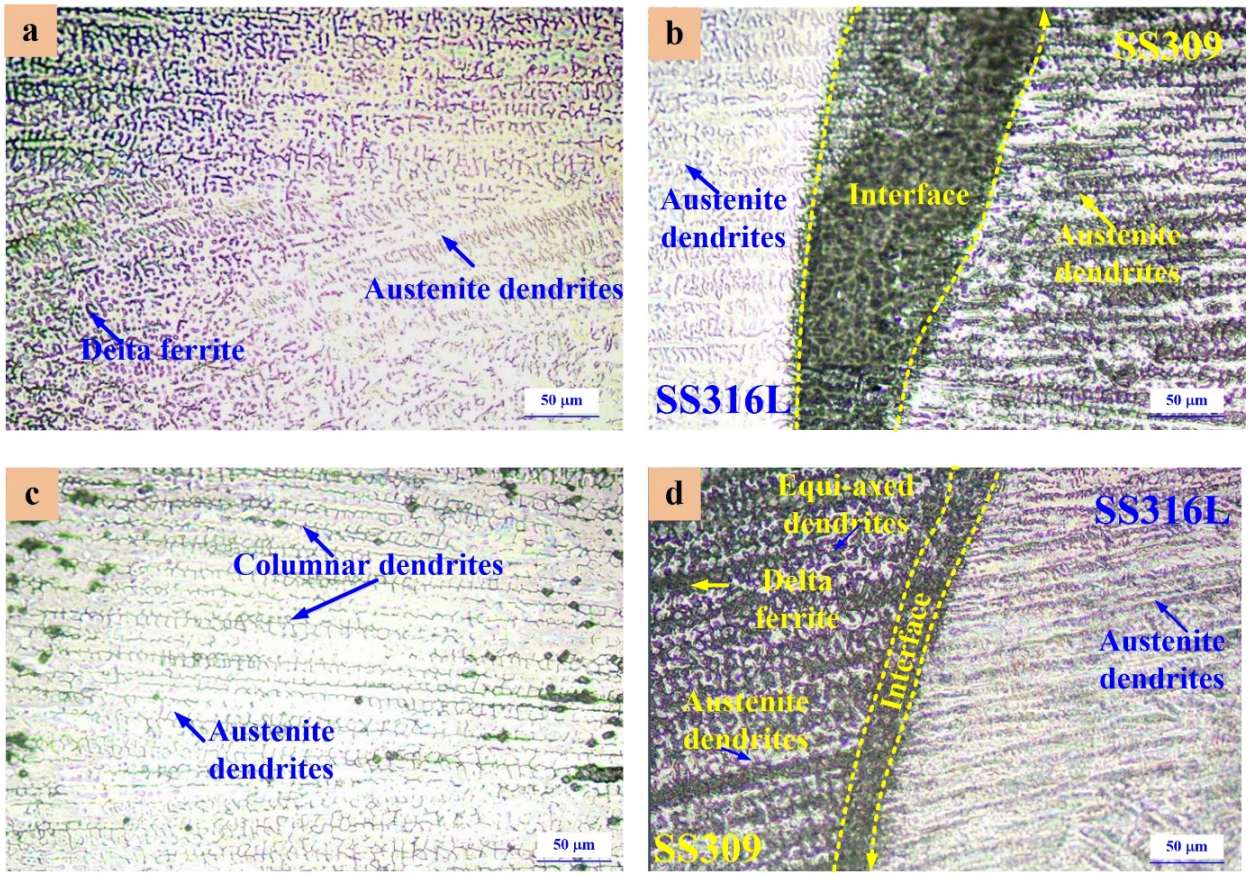


Fig. 5. Optical microscope microstructure of bimetallic sample (a) SS316L, (b) SS316L-SS309, (c) SS309, and (d) SS309-SS316L

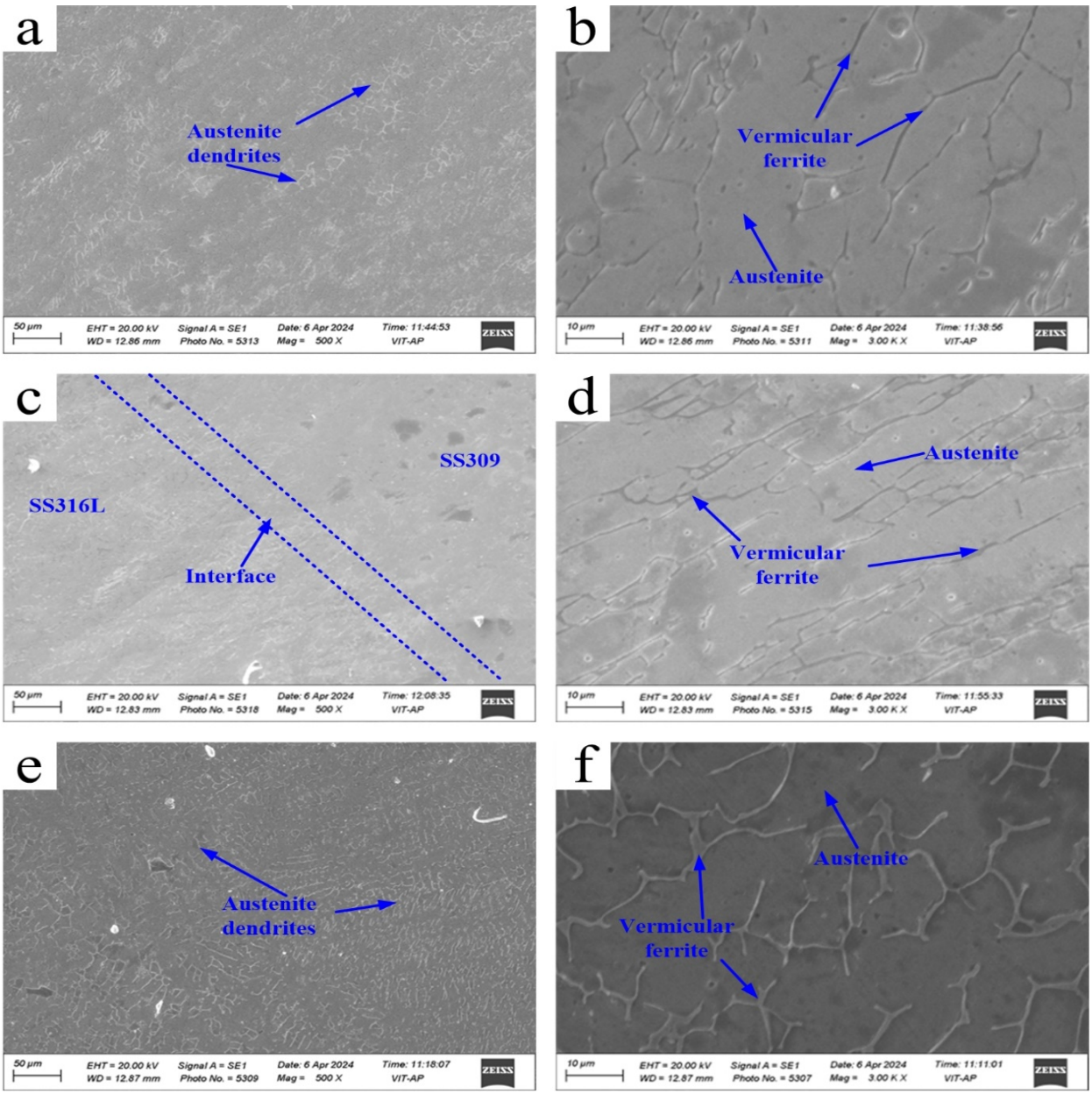


Fig. 6. SEM microstructure for bimetallic sample (a,b) SS316L, (c,d) SS309 and (e,f) SS309-SS316L interface

austenitic FCC phase as the primary microstructural constituent, consistent with the JCPDS reference file 33-0397 for austenitic stainless steel. Notably, the BMS sample exhibits an additional low-intensity peak at (110), characteristic of a ferritic BCC phase. Peaks at (110), (200), and (211), typically associated with ferritic structures, are commonly observed in stainless steels subjected to rapid cooling rates and steep thermal gradients – conditions inherent to Wire Arc DED processes. This observation aligns with the JCPDS reference file 06-0696 for the ferrite phase. The emergence of ferrite in the bimetallic sample is particularly significant and can be attributed to the compositional disparity between SS316L and SS309. The higher chromium content in SS309 promotes ferrite stabilization, leading to the development of a dual-phase microstructure comprising both FCC and BCC phases at the SS316L-SS309 interface. This dual-phase configuration, resulting from localized thermal cycles and compositional

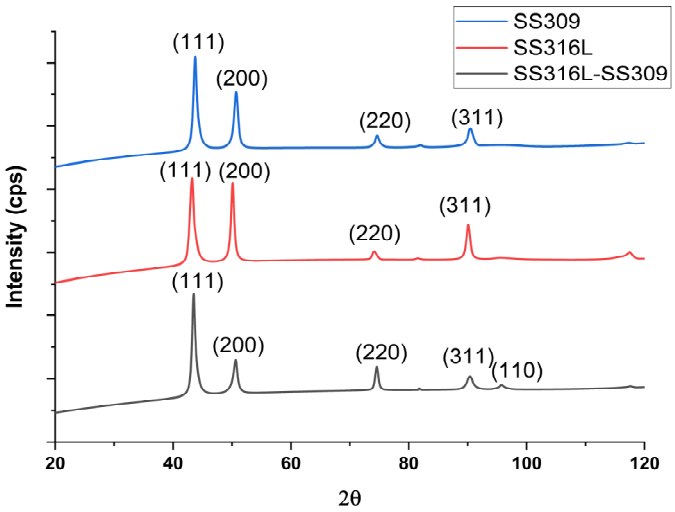


Fig. 7. XRD analysis of BMS

gradients, enhances the performance of the fabricated structure by improving resistance to solidification cracking and bolstering high-temperature mechanical properties. The detection of ferrite in the BMS is a critical finding, highlighting the complex interplay between thermal cycling, compositional variations, and microstructural evolution. This insight provides a foundation for optimizing the process and improving the mechanical integrity and thermal resilience of Wire Arc DED-fabricated bimetallic components.

### 3.3. SEM results after heat treatment

The SEM analysis of the SS316L-SS309 bimetallic WAAM samples subjected to heat treatment at 400°C, 950°C, and 1200°C for 2 hours, followed by water quenching, reveals distinct microstructural changes across the SS316L region, the interface, and the SS309 region shows in Fig. 8(a-i). In the as-deposited SS316L sample, $\delta$-ferrite dendrites are dispersed within an austenitic matrix. Upon heat treatment at 400°C, the $\delta$-ferrite dendrites exhibit increased thickness, indicating a coarsening effect due to the thermal exposure. Image analysis shows that the $\delta$-ferrite content is highest at this temperature, with the dendrites being significantly larger compared to other conditions. However, at 950°C, there is a notable reduction in both the size and content of the $\delta$-ferrite, with the dendrites becoming finer and more homogeneously distributed. The deviation in dendrite size observed in the as-deposited state is reduced at this higher temperature. At 1200°C, the $\delta$-ferrite content decreases further, and the dendrites are significantly smaller, reflecting the effects of high-temperature exposure and subsequent rapid cooling from water quenching. The interface between SS316L and SS309 shows considerable microstructural variation with temperature. At 400°C, the interface thickness is approximately 500 µm, indicating limited diffusion. As the temperature increases to 950°C, the interface thickness reduces significantly, measuring around 28 µm, suggesting enhanced diffusion and homogenization between the two dissimilar metals. At 1200°C, grain coarsening is observed at the interface due to the elevated thermal exposure, which promotes grain growth and reduces the interface thick-

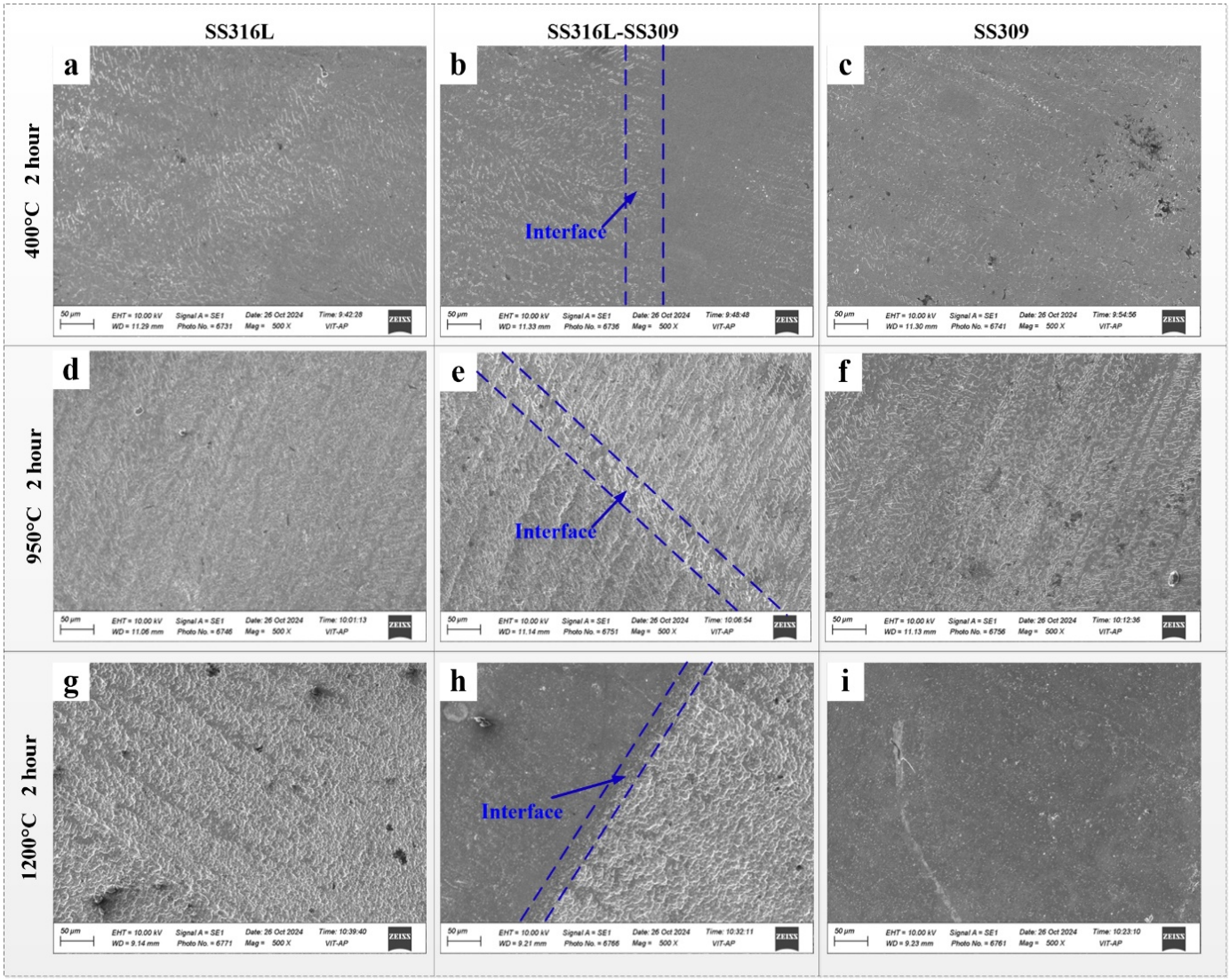


Fig. 8. SEM microstructure of SS316L, SS316L-SS309 and SS309 after heat treatment (a,b,c) at 400°C, (d,e,f) at 950°C and (g,h,i) at 1200°C each for 2 hours

ness. The rapid cooling from water quenching further influences the microstructural refinement at these elevated temperatures. The SS309 region displays distinct features in response to heat treatment. The SEM images at 400°C reveal elongated $\delta$-ferrite structures within the austenitic matrix, with the $\delta$-ferrite content being higher than in SS316L due to its alphageneous element composition. At 950°C, while the $\delta$-ferrite remains elongated, there is a slight reduction in its size, consistent with the overall decrease in $\delta$-ferrite observed in the SS316L side. Interestingly, at 1200°C, the elongated $\delta$-ferrite structures persist, but with more refined and smaller grain sizes, possibly due to the rapid cooling effect of water quenching, which inhibits further coarsening. Unlike SS316L, the SEM images for all heat-treated SS309 samples show no signs of etching pits or porosity, confirming the integrity of the microstructure across all conditions.

### 3.4. Microhardness of BMS

The microhardness profile of the SS316L-SS309 bimetallic WAAM samples, subjected to heat treatments at 400°C, 950°C, and 1200°C for 2 hours followed by water quenching, reveals distinct variations in hardness across the SS316L region, the interface, and the SS309 region, as shown in Fig. 9. These changes in microhardness are closely related to the microstructural transformations induced by the heat treatments. In the as-deposited condition, the SS316L side exhibits a relatively homogeneous microhardness distribution, which aligns with the typical hardness values reported for WAAM-fabricated austenitic stainless steels [26]. The presence of $\delta$-ferrite dendrites embedded within the austenite matrix contributes to its overall hardness. Upon heat treatment at 400°C for 2 hours, the microhardness remains comparable to the as-deposited condition, with only a slight increase near the interface due to the coarsening of $\delta$-ferrite dendrites. However, at 950°C, a significant decrease in microhardness is observed throughout the SS316L region. This reduction can be attributed to the dissolution of $\delta$-ferrite into the austenite matrix, resulting in a softer, more uniform microstructure. At 1200°C, further reduction in hardness is noted, likely due to extensive grain growth and the reduction of residual stresses facilitated by the high-temperature exposure and subsequent water quenching. The interface between SS316L and SS309 consistently shows the highest microhardness across all samples, particularly at 400°C and 950°C heat treatments. The 400°C-2 h sample demonstrates the highest hardness peak at the interface, which is attributed to the retention of δ-ferrite and fine intermetallic phases formed due to limited diffusion at this moderate temperature. The 950°C-2 h sample also exhibits elevated hardness at the interface, though slightly lower than the 400°C-treated sample. This can be linked to partial dissolution of δ-ferrite and interfacial homogenization, reducing the hardness compared to the lower temperature treatment. By 1200°C, the interfacial hardness decreases significantly due to enhanced diffusion and grain coarsening, resulting in a more uniform hardness profile across the interface. On the SS309 side, the microhardness trends differ significantly. In the as-deposited condition, the SS309 region exhibits hardness levels that are consistent with previous reports for WAAM-processed austenitic stainless steels, particularly near the interfacial zone where strain hardening and phase transformations contribute to increased hardness. After heat treatment at 400°C, the SS309 region shows a marked increase in hardness, especially near the interface, due to the formation of elongated $\delta$-ferrite structures enriched with alphagenous elements (e.g., Cr, Mo), which stabilize the ferrite phase. At 950°C, although there is a slight decrease in hardness, it remains higher than the SS316L side, attributed to the stability of $\delta$-ferrite in SS309 and the retention of finer

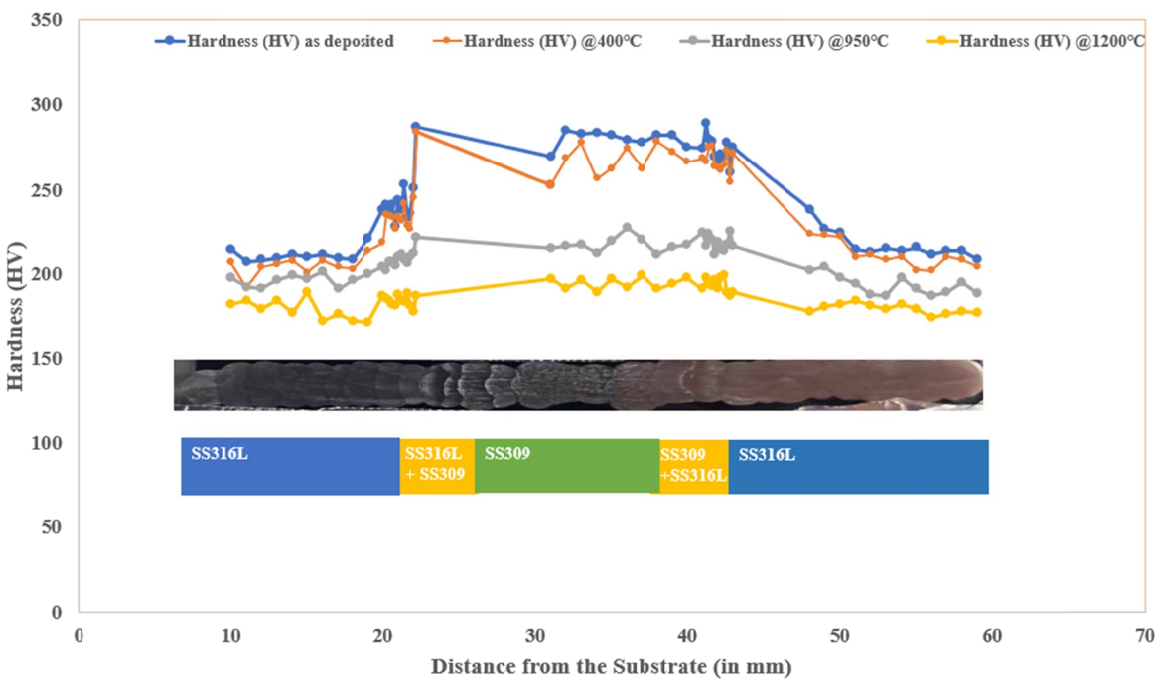


Fig. 9. Microhardness of BMS heat treated sample

dendritic structures. Conversely, the 1200°C heat treatment leads to a reduction in microhardness across the SS309 region due to grain coarsening and the reduction of dislocation density from high-temperature exposure and subsequent rapid quenching. Nevertheless, the hardness values generally stabilize between 180 to 220 HV, indicating that SS309 maintains its mechanical integrity even at elevated temperatures.

### 3.5. Tensile results of the heat-treated samples

The heat treatment at 950°C and 1200°C achieved a significant enhancement in mechanical properties shown in Fig. 10. The as-deposited samples exhibited a tensile strength (UTS) of 671 MPa and an elongation of 53.5%. In comparison, the samples treated at 400°C for 2 hours and as deposited showed a UTS of 626 MPa with an elongation of 52.7%, reflecting only marginal improvements. However, the 950°C-2 hour treatment resulted in a UTS of 577 MPa and an elongation of 62.6%, indicating substantial gains in ductility and toughness. Notably, the heat treatment at 1200°C achieved the most pronounced improvements, with a UTS of 649 MPa and a remarkable elongation of 93.1%, nearly doubling the ductility compared to the as-deposited condition. The observed enhancement in mechanical strength and ductility is primarily attributed to the microstructural refinement on both the SS316L and SS309 sides. At 950°C, the elimination of grain growth and softening on the SS309 side, along with the reduction in $\delta$-ferrite on the SS316L side, contributed to the superior mechanical performance. In contrast, while the 400°C treatment resulted in similar properties to the as-deposited condition, repeated testing confirmed that the 950°C heat treatment produced more consistent and reliable results. These findings are further corroborated by the stress-strain curves, which depict the progressive improvement in mechanical properties with increasing heat treatment temperatures. The transformation from a ferritic to a predominantly austenitic structure with reduced $\delta$-ferrite content is key to achieving the optimal balance of strength and ductility in the SS316L/SS309 bimetallic WAAM structure.

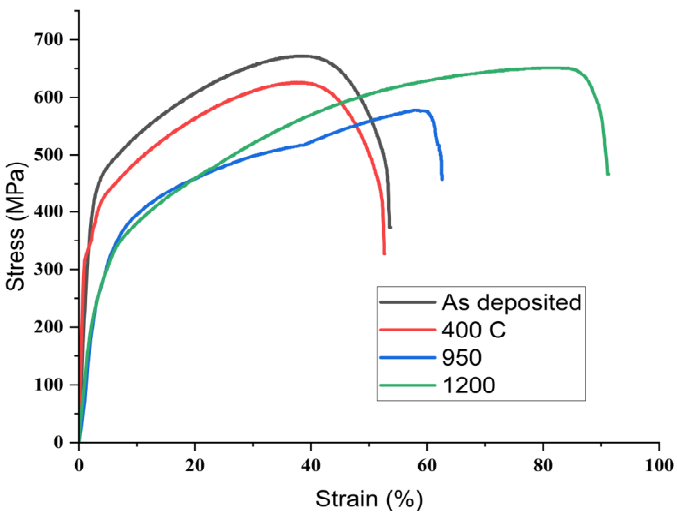


Fig. 10. Engineering Stress-Strain curve for BMS heat treated sample

### 3.6. Failure and fractography analysis

The SEM images of the fracture surfaces, as presented in Fig. 11, reveal distinct dimple morphologies characteristic of ductile fracture modes. In the samples subjected to heat treatment at 400°C, 950°C, and 1200°C for 2 hours, the fracture surface (see Fig. 11(a-f)) displays elongated dimples along the edges, indicative of localized shearing. These features are consistent with a shear-dominated deformation mechanism, suggesting that the material experienced a combination of tensile and shear stresses during fracture. However, upon closer examination of the central region of these fracture surfaces, cup-like equiaxed dimples are observed. These uniformly distributed dimples are typical of a ductile fracture under pure tensile loading, indicating that the central portion of the sample failed primarily due to tensile stress. The presence of these dimple features, both elongated and equiaxed, suggests a highly ductile failure mode across the entire cross-section of the sample. The absence of brittle fracture indicators, such as cleavage facets or intergranular cracking, confirms that the failure mode remained purely ductile, regardless of proximity to the bimetallic interface or the SS309 side. This observation holds true across all heat treatment conditions examined, from 400°C to 1200°C. For samples treated at higher temperatures, particularly at 950°C and 1200°C, the SEM analysis revealed a more uniform distribution of equiaxed dimples across the fracture surface. These features are indicative of enhanced ductility, likely due to the homogenization of microstructural phases and reduction in δ-ferrite content. The increased austenite fraction on the SS316L side and the refined microstructure on the SS309 side contributed to this ductile behavior. Moreover, no evidence of crack propagation into the interface region or transition into the SS309 side was detected, suggesting a strong metallurgical bond between the dissimilar metals in the WAAM structure. At 950°C and 1200°C both small dimples and elongated dimples are observed on the fracture surface. The size of dimples increases with temperature whereas density of it decreases. The fracture consistently occurred within the SS316L side, particularly in regions with reduced hardness, as previously noted in the microhardness profiles. In summary, the fractographic examination corroborates the tensile test results, confirming that all samples exhibited a ductile fracture mechanism characterized by dimple rupture. The elongated dimples along the edges and equiaxed dimples at the center signify a combination of shear and tensile stress distribution during failure. This behavior is consistent across the as-deposited and heat-treated conditions, indicating that the bimetallic WAAM structures maintain ductile integrity even after various thermal exposures.

## 4. Conclusion

This study comprehensively evaluated the influence of post-WAAM heat treatments on the microstructural and mechanical properties of SS316L-SS309 thin wall austenitic steel (BMS).

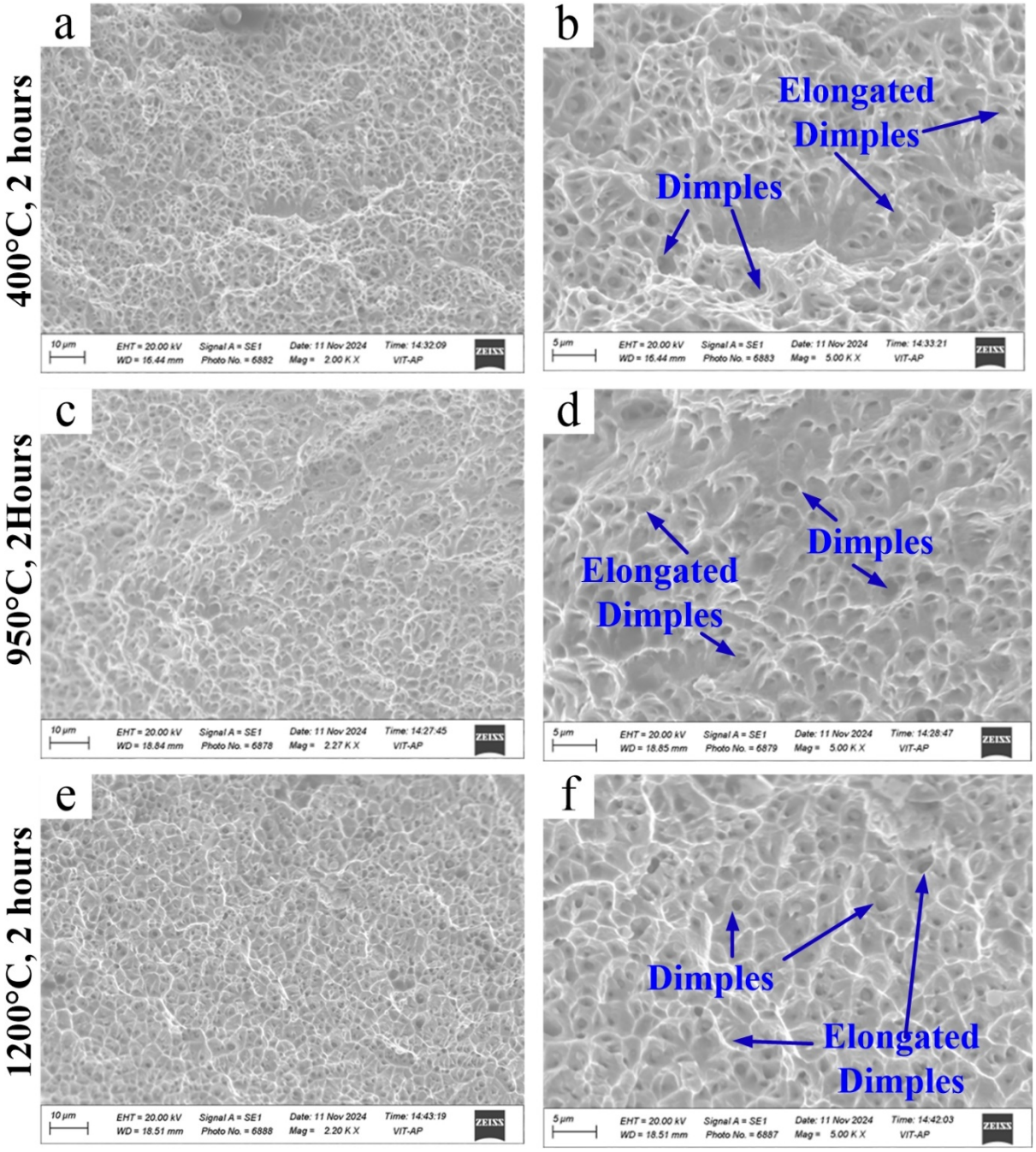


Fig. 11. Fractured surfaces SEM images of BMS heat treated sample (a,b) at 400°C (c,d) at 950°C, and (e,f) at 1200°C

1. The as-deposited WAAM specimens exhibited an austenitic dendritic structure with a mixture of δ-ferrite and austenite phases.
2. The mechanical properties of the as-built samples demonstrated a yield strength (YS) of 383 MPa, ultimate tensile strength (UTS) of 558 MPa, and a maximum elongation of 60%. Notably, the highest hardness was recorded at the interface region of the as-deposited samples.
3. Upon heat treatment at 400°C, the microstructure remained largely unchanged, with characteristics similar to those of the as-deposited condition, indicating that this stress relief temperature had a minimal impact on phase transformation and mechanical properties.
4. At 950°C, no significant morphological alterations were observed; however, a 14.3% at 950°C in UTS was noted, accompanied by a marginal increase in elongation (approximately 1.5% higher than the as-deposited sample).
5. At 950°C and 1200°C both small dimples and elongated dimples are observed on the fracture surface. The size of dimples increases with temperature whereas density of it decreases.
6. A substantial transformation occurred at 1200°C, where two hours of exposure led to a complete $\delta \rightarrow \sigma$ phase transformation. This resulted in a noticeable decrease in hardness by approximately 25-35 HV, particularly on the SS309 side, due to the inherently softer austenitic matrix.

The mechanical properties were adversely affected at this elevated temperature, with a significant reduction in UTS, while elongation doubled in comparison to the as-deposited condition.

These findings highlight the critical role of heat treatment parameters in tailoring the microstructure and mechanical behaviour of WAAM-fabricated SS316L-SS309 bimetallic structures, providing valuable insights for optimizing their performance in demanding applications.

The study highlights the limitations of WAAM-fabricated samples in maintaining mechanical properties and microstructural stability at elevated temperatures, particularly at 1200°C, where the $\delta \rightarrow \sigma$ phase transformation significantly degraded material performance. Additionally, the minimal impact of heat treatment at 400°C indicates limited scope for stress relief optimization. Future work should focus on enhancing the thermal stability of WAAM components through alloy modifications or tailored heat treatment protocols. Investigations into alternative phase transformation pathways and their effects on mechanical properties can further advance the applicability of WAAM-fabricated materials for high-temperature applications.

**Acknowledgement**

The authors would like to acknowledge the financial support provided by the Science and Engineering Research Board (SERB), Department of Science and Technology (DST), Government of India, under Project File No. CRG/2022/003042. We also express our sincere gratitude to VIT-AP University for providing the required allied facilities for this research.

## REFERENCES

[1] E. Hosseini, V. A. Popovich, A review of mechanical properties of additively manufactured Inconel 718. Addit. Manuf. **30**, 100877 (2019).
DOI: https://doi.org/10.1016/j.addma.2019.100877

[2] T. DebRoy et al., Additive manufacturing of metallic components – Process, structure and properties. Prog. Mater. Sci. **92**, 112-224 (2018). DOI: https://doi.org/10.1016/j.pmatsci.2017.10.001

[3] Jhavar, Suyog, Wire arc additive manufacturing: approaches and future prospects. Additive Manufacturing. Woodhead Publishing, 183-208 (2021).
DOI: https://doi.org/10.1016/B978-0-12-822056-6.00004-7

[4] S. M. Thompson, L. Bian, N. Shamsaei, A. Yadollahi, An overview of Direct Laser Deposition for additive manufacturing; Part I: Transport phenomena, modeling and diagnostics. Addit. Manuf. **8**, 36-62 (2015).
DOI: https://doi.org/10.1016/j.addma.2015.07.001

[5] A. Bandyopadhyay, Y. Zhang, S. Bose, Recent developments in metal additive manufacturing. Curr. Opin. Chem. Eng. **28**, 96-104 (2020).
DOI: https://doi.org/10.1016/j.coche.2020.03.001

[6] D. Wang et al., Recent progress on additive manufacturing of multi-material structures with laser powder bed fusion. Virt. Phys. Prototyp. **17**, 329-365 (2022).
DOI: https://doi.org/10.1080/17452759.2022.2028343

[7] Ahn, Dong-Gyu, Directed energy deposition (DED) process: state of the art. Int. J. Precis. Eng. Manuf.-Green Technol. **8.2**, 703-742 (2021). DOI: https://doi.org/10.1007/s40684-020-00302-7

[8] N. Kladovasilakis, P. Charalampous, I. Kostavelis, D. Tzetzis, D. Tzovaras, Impact of metal additive manufacturing parameters on the powder bed fusion and direct energy deposition processes: a comprehensive review. Prog. Addit. Manuf. **6**, 349-365 (2021).
DOI: https://doi.org/10.1007/s40964-021-00180-8

[9] M.R.U. Ahsan et al., Microstructures and mechanical behavior of the bimetallic additively-manufactured structure (BAMS) of austenitic stainless steel and Inconel 625. J. Mater. Sci. Technol. **74**, 176-188 (2021).
DOI: https://doi.org/10.1016/j.jmst.2020.10.001

[10] M. Srivastava, S. Rathee, A. Tiwari, M. Dongre, Wire arc additive manufacturing of metals: A review on processes, materials and their behaviour. Mater. Chem. Phys. **294**, 126988 (2023).
DOI: https://doi.org/10.1016/j.matchemphys.2022.126988

[11] R. Singh Tanwar, S. Jhavar, Ti based alloys for aerospace and biomedical applications fabricated through wire + arc additive manufacturing (WAAM). Mater. Today Proc. **98**, 226-232 (2024).
DOI: https://doi.org/10.1016/j.matpr.2023.11.121

[12] H. Ding, B. Zou, X. Wang, J. Liu, L. Li, Microstructure , mechanical properties and machinability of 316L stainless steel fabricated by direct energy deposition. Int. J. Mech. Sci. **243**, 108046 (2022).
DOI: https://doi.org/10.1016/j.ijmecsci.2022.108046

[13] C. Nota, G. Rückert, J. Heuzé, et al., A first feedback on manufacturing and in-service behaviour of a WAAM-made propeller for naval application. Weld World **67**, 1113-1121 (2023).
DOI: https://doi.org/10.1007/s40194-023-01475-w

[14] American Welding Society (AWS), Structural Welding Code – Stainless Steel. Am. Weld. Soc., [Online]. Available: https://pubs.aws.org/Download_PDFS/D1.6-D1.6M-2007PV.pdf

[15] B.O. Okonkwo, H. Ming, J. Wang, F. Meng, X. Xu, Microstructural characterization of low alloy steel A508 – 309 / 308L stainless steel dissimilar weld metals. Int. J. Press. Vessels Pip. **190**, 104297 (2021). DOI: https://doi.org/10.1016/j.ijpvp.2020.104297

[16] R. Chaudhari, S. Khanna, J. Vora, V. Patel, Experimental investigations on microstructure and mechanical properties of wall structure of SS309L using wire-arc additive manufacturing. J. Adv. Join. Process. **9**, 100172, Jun. (2024).
DOI: https://doi.org/10.1016/j.jajp.2023.100172

[17] C. Guo, S. Shi, J. Yu, S. Zhang, H. Dai, Addressing the strength-corrosion tradeoff in 316 L stainless steel by introducing cellular ferrite via directed energy deposition. Addit. Manuf. **86**, 104201, (2024). DOI: https://doi.org/10.1016/j.addma.2024.10420

[18] Chhibber, Rahul, Navneet Arora, B.K. Dutta, Residual stresses in bimetallic weld joint with varying buttering layer thickness. International Manufacturing Science and Engineering Conference. **51364**. American Society of Mechanical Engineers (2018).
DOI: https://doi.org/10.1115/msec2018-6729

[19] S. Guo et al., Microstructure and mechanical properties of high nitrogen steel – high strength steel bimetallic multi-layered steels fabricated by plasma-arc additive manufacturing. Mater. Today Commun. **37**, 107538 (2023).
DOI: https://doi.org/10.1016/j.mtcomm.2023.107538

[20] H. Ban, X. Yang, Y. Shi, K. Chung, Y. Hu, Micro-macro properties of stainless-clad bimetallic steel welded connections with different configurations. J. Constr. Steel Res. **217**, 108637 (2024).
DOI: https://doi.org/10.1016/j.jcsr.2024.108637

[21] W. Wu et al., Current-Carrying Wear Behavior of Bi-Containing Graphite / Copper-Matrix Composites via Hot Powder Forging. J. Mater. Eng. Perform. **33**, 1560-1571 (2024).
DOI: https://doi.org/10.1007/s11665-023-08090-2

[22] G. Li et al., Preparation, interfacial regulation and strengthening of Mg / Al bimetal fabricated by compound casting: A review. J. Magnes. Alloys **11**, 3059-3098 (2023).
DOI: https://doi.org/10.1016/j.jma.2023.09.001

[23] Tang, Zhaofeng, et al., Interface microstructure regulation and bonding performance of powder metallurgy Al/Mg bimetal with Ni interlayer. J. Mater. Sci. **58**, 13, 5848-5864 (2023).
DOI: https://doi.org/10.1007/s10853-023-08362-1

[24] S.V. Motghare, K.M. Ashtankar, N.K. Lautre, Experimental investigation of electrochemical and mechanical properties of stainless steel 309L at different built orientation by cold metal transfer assisted wire arc additive manufacturing. Mater. Today Commun. **39**, 109382 (2024).
DOI: https://doi.org/10.1016/j.mtcomm.2024.109382

[25] X. Chen, J. Li, X. Cheng, H. Wang, Z. Huang, Effect of heat treatment on microstructure, mechanical and corrosion properties of austenitic stainless steel 316L using arc additive manufacturing. Mater. Sci. Eng. A. **715**, 307-314 (2018).
DOI: https://doi.org/10.1016/j.msea.2017.10.002

[26] Chen, Nan, et al., Enhancement of an additive-manufactured austenitic stainless steel by post-manufacture heat-treatment. Mater. Sci. Eng. A. **759**, 65-69 (2019).
DOI: https://doi.org/10.1016/j.msea.2019.04.111

[27] T.A. Rodrigues et al., Effect of heat treatments on 316 stainless steel parts fabricated by wire and arc additive manufacturing: Microstructure and synchrotron X-ray diffraction analysis. Addit. Manuf. **48**, 102428 (2021).
DOI: https://doi.org/10.1016/j.addma.2021.102428

[28] V. Kumar, S. Dwivedi, A. Mandal, A.R. Dixit, Experimental investigations on the microstructural evolution and their influence on mechanical , tribological and corrosion performance of wire-arc additive manufactured SS316L structure. Mater. Today Commun. **38**, 107673 (2023).
DOI: https://doi.org/10.1016/j.mtcomm.2023.107673

[29] R.U. Ahsan, A. Newaz, M. Tanvir, T. Ross, A. Elsawy, Fabrication of bimetallic additively manufactured structure ( BAMS ) of low carbon steel and 316L austenitic stainless steel with wire arc additive manufacturing. Rapid Prototyp. J. **3**, 519-530 (2020).
DOI: https://doi.org/10.1108/rpj-09-2018-0235

[30] S. Kesarwani, N. Yuvaraj, M.S. Niranjan, Impact of depositional direction and current on microstructure and mechanical properties of the bimetallic wall of ER5356 / ER4043 fabricated by cold metal transfer based wire arc additive manufacturing. CIRP J. Manuf. Sci. Technol. **53**, 17-33 (2024).
DOI: https://doi.org/10.1016/j.cirpj.2024.06.013